We are IntechOpen,
the world's leading publisher of Open Access books
Built by scientists, for scientists

6,900
Open access books available

186,000
International authors and editors

200M
Downloads

154
Countries delivered to

Our authors are among the

TOP 1%
most cited scientists

12.2%
Contributors from top 500 universities

CLARIVATE ANALYTICS
BOOK CITATION INDEX
INDEXED

WEB OF SCIENCE™

Selection of our books indexed in the Book Citation Index
in Web of Science™ Core Collection (BKCI)

Interested in publishing with us?
Contact book.department@intechopen.com

Mechanical Properties of Biomaterials Based on Calcium Phosphates and Bioinert Oxides for Applications in Biomedicine

Siwar Sakka, Jamel Bouaziz and Foued Ben Ayed

1. Introduction

Calcium phosphates (CaP) have been sought as biomaterials for reconstruction of bone defect in maxillofacial, dental and orthopaedic applications [1-31]. Calcium phosphates have been used clinically to repair bone defects for many years. Calcium phosphates such as hydroxyapatite ($Ca_{10}(PO_4)_6(OH)_2$, HAp), fluorapatite ($Ca_{10}(PO_4)_6F_2$, FAp), tricalcium phosphate ($Ca_3(PO_4)_2$, TCP), TCP-HAp composites and TCP-FAp composites are used for medical and dental applications [3, 10-29]. In general, this concept is determined by advantageous balances of more stable (frequent by hydroxyapatite or fluorapatite) and more resorbable (typically tricalcium phosphate) phases of calcium phosphates, while the optimum ratios depend on the particular applications. The complete list of known calcium phosphates, including their major properties (such, the chemical formula, solubility data) is given in Table 1. The detailed information about calcium phosphates, their synthesis, structure, chemistry, other properties and biomedical applications have been comprehensively reviewed recently in reference [24].

Calcium phosphate-based biomaterials and bioceramics are now used in a number of different applications throughout the body, covering all areas of the skeleton. Applications include dental implants, percutaneous devices and use in periodontal treatment, treatment of bone defects, fracture treatment, total joint replacement (bone augmentation), orthopedics, cranio-maxillofacial reconstruction, otolaryngology and spinal surgery [32-35]. Depending upon whether a bioresorbable or a bioactive material is desired, different calcium orthophosphates might be used.

INTECH
open science | open minds

In the past, many implantations failed because of infection or a lack of knowledge about the toxicity of the selected materials. In this frame, the use of calcium phosphates is logical due to their similarity to the mineral phase of bone and teeth [36-40]. However, according to available literature, the first attempt to use calcium phosphates as an artificial material to repair surgically-created defects in rabbits was performed in 1920 [41]. More than fifty years later, the first dental application of a calcium phosphate (erroneously described as TCP) in surgically-created periodontal defects [42] and the use of dense HAp cylinders for immediate tooth root replacement were reported [43]. Since Levitt et al. described a method of preparing an apatite bioceramics from FAp and suggested its possible use in medical applications in 1969[44]. According to the available databases, the first paper with the term ''bioceramics'' in the abstract was published in 1971 [45], while those with that term in the title were published in 1972 [46-47]. However, application of ceramic materials as prostheses had been known before [48-49]. Further historical details might be found in literature [50]. Commercialization of the dental and surgical applications of Hap-based bioceramics occurred in the 1980's, largely through the pioneering efforts by Jarcho [51], de Groot [52] and Aoki [53]. Due to that, HAp has become a bioceramic of reference in the field of calcium phosphates for biomedical applications. Preparation and biomedical applications of apatites derived from sea corals (coralline HAp) [54–56] and bovine bone were reported at the same time [57]. Since 1990, several other calcium phosphate cements have been developed [58-62], injectable cements have been formulated [63], and growth factors have been delivered via these cements [64]. The tetracalcium phosphate [TTCP: $Ca_4(PO_4)_2O$] and dicalcium phosphate anhydrous [DCPA: $CaHPO_4$] system was approved in 1996 by the Food and Drug Administration (FDA) for repairing craniofacial defects in humans, thus becoming the first TTCP–DCPA system for clinical use [65]. However, due to its brittleness and weakness, the use of TTCP–DCPA system was limited to the reconstruction of non-stress-bearing bone [66-67]. To expand the use of TTCP–DCPA system to a wide range of load-bearing maxillofacial and orthopedic repairs, recent studies have developed natural biopolymers that are elastomeric, biocompatible and resorbable [68]. Calcium phosphates in a number of forms and compositions are currently either in use or under consideration in many areas of dentistry and orthopedics. For example, bulk materials, available in dense and porous forms, are used for alveolar ridge augmentation, immediate tooth replacement and maxillofacial reconstruction [35, 69]. Other examples include orbital implants (Bio-Eye) [70-71], increment of the hearing ossicles, spine fusion and repair of bone defects [72-73]. In order to permit growth of new bone onto bone defects, a suitable bioresorbable material should fill the defects. Otherwise, in-growth of fibrous tissue might prevent bone formation within the defects [69-73]. Today, a large number of different calcium phosphate bioceramics for the treatment of various defects are available on the market.

The performance of living tissues is the result of millions of years of evolution, while the performance of acceptable artificial substitutions those man has designed to repair damaged hard tissues are only a few decades old. Archaeological findings exhibited in museums showed that materials used to replace missing human bones and teeth have included animal or human (from corpses) bones and teeth, shells, corals, ivory (elephant tusk), wood, as well as some metals (gold or silver). For instance, the Etruscans learned to substitute missing

teeth with bridges made from artificial teeth carved from the bones of oxen, while in ancient Phoenicia loose teeth were bound together with gold wires for tying artificial ones to neighboring teeth.

Compound	Acronym	Formula	Ca/P	pK$_s$[a]
Monocalcium phosphate monohydrate	MCPM	$Ca(H_2PO_4)_2 .H_2O$	0.5	1.14
Monocalcium phosphate anhyrous	MCPA	$Ca(H_2PO_4)_2$	0.5	1.14
Dicalcium phosphate dihydrate	DCPD	$CaHPO_4 .2H_2O$	1	6.59
Dicalcium phosphate anhydrous	DCPA	$CaHPO_4$	1	6.90
Aporphous calcium phosphates	ACP	$Ca_xH_y(PO_4)_z .nH_2O$ n = 3-4.5; 12-20%H_2O	1.2-2.2	b
Octacalcium phosphate	OCP	$Ca_8(HPO_4)_2(PO_4)_4 .5H_2O$	1.33	96.6
α- Tricalcium phosphate	α-TCP	α- $Ca_3(PO_4)_2$	1.5	25.5
β- Tricalcium phosphate	β-TCP	β- $Ca_3(PO_4)_2$	1.5	28.9
Calcium-deficient Hydroxyapatite	CDHAp	$Ca_{10-x}(HPO_4)_x(PO_4)_{6-x}(OH)_{2-x}$ (0 < x < 1)	1.5-1.67	85
Hydroxyapatite	HAp	$Ca_{10}(PO_4)_6(OH)_2$	1.67	116.8
Fluorapatite	FAp	$Ca_{10}(PO_4)_6F_2$	1.67	120
Oxapatite	OAp	$Ca_{10}(PO_4)_6O$	1.67	69
Tetracalcium phosphate	TTCP	$Ca_4(PO_4)_2O$	2	38-44

[a]: Solubility at 25°C (pK$_s$ = -logK$_s$);

[b] : Cannot be measured precisely.

Table 1. Calcium phosphates and their major properties [3, 24]

Calcium phosphates are established materials for the augmentation of bone defects. They are available as allogenic, sintered materials. Unfortunately, these calcium phosphates exhibit relatively poor tensile and shear properties [74]. In practice, the strength of the calcium phosphate cements is lower than that of bone, teeth, or sintered calcium phosphate bioceramics [75] and, together with their inherent brittleness, restricts their use to non-load bearing defects [76] or pure compression loading [74]. Typical applications are the treatment of maxillo-facial defects or deformities [77] and cranio facial repair [78] or augmentation of spine and tibial plateau [74]. A successful improvement of the mechanical properties would significantly extend the applicability of calcium phosphates [79] and can be achieved by forming composite materials [80]. Second phase additives to the calcium phosphate composites have been either fibrous reinforcements or bioinert oxides that interpenetrate the porous matrix.

Hydroxyapatite and other calcium phosphates bioceramics are important for hard tissue repair because of their similarity to the minerals in natural bone, and their excellent biocompatibility and bioactivity [81-86]. When implanted in an osseous site, bone bioactive materials such as HAp and other CaP implants and coatings provide an ideal environment for cellular reaction and colonization by osteoblasts. This leads to a tissue response termed osteoconduction in which bone grows on and bonds to the implant, promoting a functional interface [81, 84, 87]. Extensive efforts have significantly improved the properties and performance of HAp and other CaP based implants [88-92]. Calcium phosphate cements can be molded or injected to form a scaffold in situ, which can be resorbed and replaced by new bone [93, 65-67]. Chemically, the vast majority of calcium phosphate bioceramics is based on HAp, β-TCP, α-TCP and/or biphasic calcium phosphate (BCP), which is an intimate mixture of either β-TCP - HAp [94-100] or α-TCP - HAp [101-111]. The preparation technique of these calcium phosphates has been extensively reviewed in literature [1, 4, 37, 102-104]. When compared to both β- and α-TCP, HAp is a more stable phase under physiological conditions, as it has a lower solubility (Table 1) [37, 109-110]. Therefore, the BCP concept is determined by the optimum balance of a more stable phase of HAp and a more soluble TCP. Due to a higher biodegradability of the β - or α -TCP component, the reactivity of BCP increases with the TCP-HAp the increase in ratio. Thus, in vivo bioresorbability of BCP can be controlled through the phase composition [95]. As implants made of calcined HAp are found in bone defects for many years after implantation, bioceramics made of more soluble calcium phosphates is preferable for the biomedical purposes [94-110]. HAp has been clinically used to repair bone defects for many years [3]. However, Hap has poor mechanical properties [3]. Their use at high load bearing conditions has been restricted due to their brittleness, poor fatigue resistance and strength.
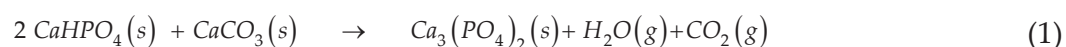
The main reason behind the use of β-TCP as bone substitute materials is their chemical similarity to the mineral component of mammalian bone and teeth [1-3]. The application of tricalcium phosphate as a bone substitute has received considerable attention, because it is remarkably biocompatible with living bodies when replacing hard tissues and because it has biodegradable properties [1-29]. Consequently, β-TCP has been used as bone graft substitutes in many surgical fields such as orthopedic and dental surgeries [3, 11-12, 16-17]. This use leads to an ultimate physicochemical bond between the implants and bone-termed osteointegration. Even so, the major limitation to the use of β-TCP as load-bearing biomaterial is their mechanical properties which make it brittle, with poor fatigue resistance [3, 10, 21-29]. Moreover, the mechanical properties of tricalcium phosphate are generally inadequate for many load-carrying applications (3 MPa – 5 MPa) [3, 10, 20-29]. Its poor mechanical behaviour is even more evident when used to make highly porous ceramics and scaffolds. Hence, metal oxides ceramics, such as alumina (Al_2O_3), titania (TiO_2) and some oxides (e.g. ZrO_2, SiO_2) have been widely studied due to their bioinertness, excellent tribological properties, high wear resistance, fracture toughness and strength as well as relatively low friction [19, 21-22, 29-31]. However, bioinert ceramic oxides having high strength are used to enhance the densification and the mechanical properties of β-TCP. In this chapter, we will try to improve the strength of β-TCP by introducing a bioinert oxide like alumina. This is because there are few articles reporting

the toughening effects of an inert oxide (like alumina (Al_2O_3)) on the mechanical properties of β-TCP [22, 27, 29]. Alumina has a high strength and is bio-inert with human tissues [19, 22, 27, 29]. In order to improve the biocompatibility of alumina and the strength of tricalcium phosphate effectively, and in order to search for an approach to produce high performances of alumina-tricalcium phosphate composites, β-TCP is introduced with different percentages in the alumina matrix. The aim of our study is to elaborate and characterize the TCP-Al_2O_3 composites for biomedical applications.

This chapter proposes to study the sintering of the alumina-tricalcium phosphate composites at various temperatures (1400°C, 1450°C, 1500°C, 1550°C and 1600°C) and with different percentages of β-TCP (10 wt%, 20 wt%, 40 wt% and 50 wt%). The characterization of biomaterials will be realized by using dilatometry analysis, differential thermal analysis (DTA), X-ray diffraction (XRD), magic angle spinning nuclear magnetic resonance (MAS NMR), scanning electron microscopy analysis (SEM) and by using the mechanical properties, such as rupture strength (σ_r) of these biomaterials.

2. Materials and methods

The synthesized tricalcium phosphate and alumina (Riedel-de Haën) were mixed in order to prepare biomaterial composites. The β-TCP powder was synthesized by solid-state reaction from calcium carbonate ($CaCO_3$) and calcium phosphate dibasic anhydrous ($CaHPO_4$) [27]. Stoichiometric amounts of high purity powders such as $CaHPO_4$ (Fluka, purity ≥ 99%) and $CaCO_3$ (Fluka, purity ≥ 98.5%), were sintered at 1000°C for one hour to obtain the β-TCP according to the following reaction:

$$2\, CaHPO_4(s) \;+\; CaCO_3(s) \quad \rightarrow \quad Ca_3(PO_4)_2(s) + H_2O(g) + CO_2(g) \tag{1}$$

The β-TCP and the alumina powders were mixed in an agate mortar. The powder mixtures were milled in ethanol for 24 hours. After milling, the mixtures were dried in a rotary vacuum evaporator and passed through a 70-mesh screen. After drying the powder mixtures at 80°C for 24 hours, they were molded in a cylinder having a diameter of 20 mm and a thickness of 6 mm, and pressed under 150 MPa. The green compacts were sintered at various temperatures for different lengths of time in a vertical furnace (Pyrox 2408). The heating rate is 10°C min^{-1}. The size of the particles of the powder was measured by means of a Micromeritics Sedigraph 5000. The specific surface area (SSA) was measured using the BET method and using N_2 as an adsorption gas (ASAP 2010) [112]. The primary particle size (D_{BET}) was calculated by assuming the primary particles to be spherical:

$$D_{BET} = 6\, /\, S\rho \tag{2}$$

where ϱ is the theoretical density and S is the surface specific area.

The microstructure of the sintered compacts was investigated using the scanning electron microscope (Philips XL 30) on the fractured surfaces of the samples. The grains' mean size was measured directly using SEM micrographs. The powder was analyzed by using Xray diffraction (XRD). The Xray patterns were recorded using the Seifert XRD 3000 TT diffractometer. The Xray radiance was produced by using CuK_α radiation ($\lambda = 1.54056$ Å). The crystalline phases were identified with the powder diffraction files (PDF) of the International Center for Diffraction Data (ICDD). Linear shrinkage was determined using dilatometry (Setaram TMA 92 dilatometer). The heating and cooling rates were 10°C min^{-1} and 20°C min^{-1}, respectively. Differential thermal analysis (DTA) was carried out using about 30 mg of powder (DTATG, Setaram Model). The heating rate was 10°C min^{-1}. The ^{31}P and ^{27}Al magic angle spinning nuclear magnetic resonance (^{31}P MAS NMR) spectra were run on a Brucker 300WB spectrometer. The ^{31}P and ^{27}Al observational frequency were 121.49 MHz and 78.2 MHz, respectively. The ^{31}P MAS-NMR chemical shifts were referenced in parts per million (ppm) referenced to 85 wt% H_3PO_4. The ^{27}Al MAS-NMR chemical shifts were referenced to a static signal obtained from an aqueous aluminum chloride solution.

The Brazilian test was used to measure the rupture strength of biomaterials [113-114]. The rupture strength (σ_r) values were measured using the Brazilian test according to the equation:

$$\sigma_r = \frac{2 \cdot P}{\Pi \cdot D \cdot t} \tag{3}$$

where P is the maximum applied load, D the diameter, t the thickness of the disc and σ_r the rupture strength (or mechanical strength).

3. Results and discussion

3.1. Characterization of different powders

The X-ray diffraction analysis of β-TCP powder and α-alumina powder are presented in Figure 1. As it can be noticed from this figure, the X-ray diffraction pattern of tricalcium phosphate powder reveals only peaks of β-TCP (ICDD data file no. 70-2065) without any other phase (Figure 1a). Consequently, the XRD pattern obtained from the alumina powder illustrates α phase peaks relative to ICDD data file no. 43-1484 (Figure 1b).

The ^{31}P MAS-NMR solid spectrum of the tricalcium phosphate powder is presented in Figure 2a. We observe the presence of several peaks of tetrahedral P sites (at 0.36 ppm, 1.46 ppm and 4.83 ppm), while there are other peaks (at -7.43 ppm, -9.09 ppm and -10.35 ppm) which reveal a low quantity of calcium pyrophosphate which was formed during the preparation of the β-TCP.

The ^{27}Al MAS-NMR solid spectrum of the alumina powder is presented in Figure 2b. We notice the presence of two peaks which are characteristic of aluminum: one peak at 7.36 ppm

corresponding to octahedral Al sites (Al^{VI}) and the other at 37.36 ppm which corresponds to pentahedral Al sites (Al^{V}). The results obtained for ^{31}P MAS-NMR and ^{27}Al MAS-NMR are similar to those previously reported by different authors [14, 22, 25-28, 31].
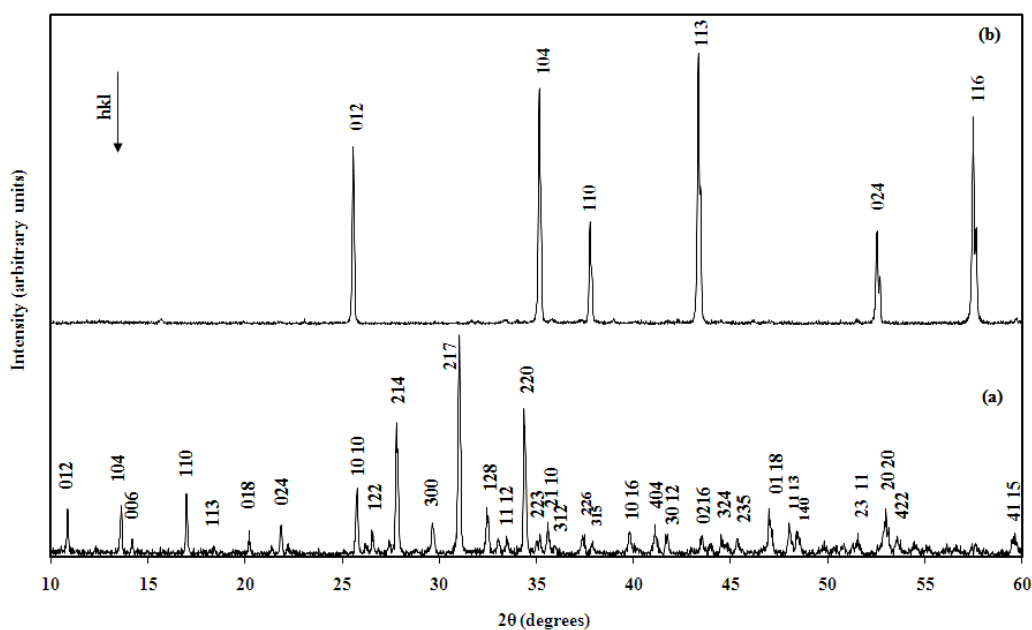

Figure 1. The XRD patterns of: (a) β-TCP powder and (b) α-Al$_2$O$_3$ powder
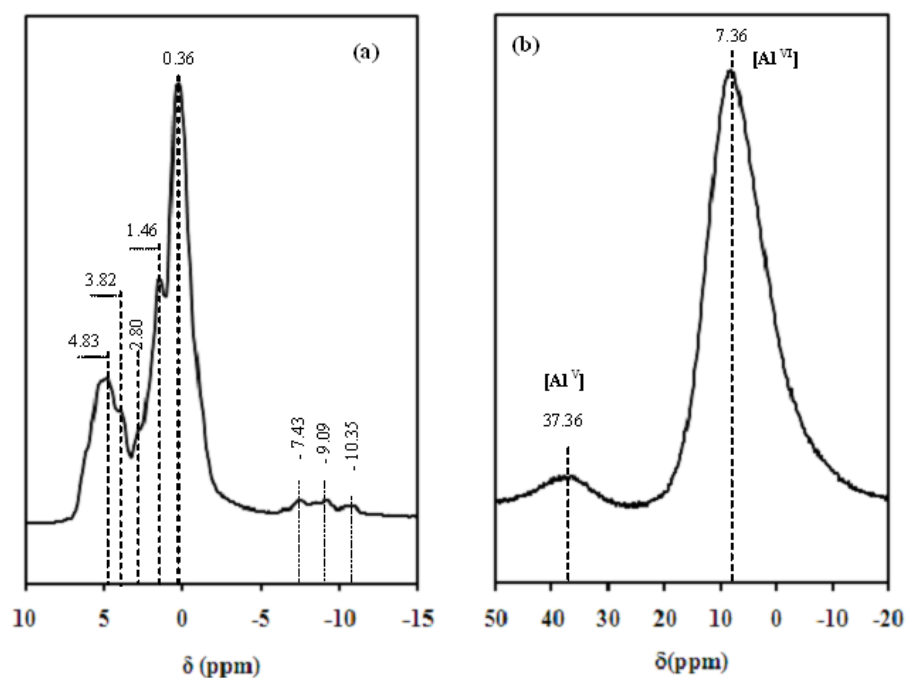

Figure 2. The ^{31}P MAS-NMR spectra of: (a) β-TCP and the ^{27}Al MAS-NMR spectra of: (b) α-Al$_2$O$_3$

The experimental characteristics of the different powders used in this study are illustrated in Table 2. Table 2 summarizes the SSA, the DTA measurements, the sintering temperature and the theoretical density of the different powders. The powder particles are assumed to be spherical; the size of the particles can be calculated using Eq. (2). The results from the average grain size obtained by the SSA (D_{BET}) and from the average grain size obtained by granulometric repartition (D_{50}) are presented in Table 2. Compared with those of the β-TCP powder, the grains of the alumina powder have a dense morphology. These (D_{BET}) values obtained by the SSA do not correspond to those obtained from the granulometric repartition (Table 2). The discrepancy may be due to the presence of agglomerates which are formed during the preparation of the β-TCP powder at 1000°C.

Compounds	SSA (m²/g) ± 1.0	D_{BET} (μm) ± 0.2	D_{50} (μm)[a] ± 0.2	DTA measurements (endothermic peak)	T(°C)[b]	d[c]
TCP	0.70	2.79	6	1100°C-1260°C (β → α)	1000 - 1300	3.070 (β)
				1470°C (α → α')		2.860 (α)
Alumina	2.87	0.53	3	-	1400 - 1600	3.98 (α)

[a] : mean diameter,

[b] : sintering temperature domain,

[c] : theoretical density

Table 2. Characteristics of the powders used in the study

Differential thermal analysis studies of the different powders used in this study detected a potential phase change during the sintering process. The DTA thermogram of β-TCP, α-Al_2O_3 and different Al_2O_3 - TCP composites are presented in Figure 3. The DTA curve of alumina reported no process relative to the sintering temperature (Figure 3a). Figure 3b shows the DTA curve of β-TCP. The DTA thermogram of β-TCP shows two endothermic peaks, relative to the allotropic transformations of tricalcium phosphate (Figure 3b). The peak between 1100°C – 1260°C is related to the first allotropic transformation of TCP (β to α), while the last peak at 1470°C is related to the second allotropic transformation of TCP (α to α'). As a matter of fact, this result is similar to the result previously reported by Destainville et al. and Ben Ayed et al. [9, 14]. Figure 3c shows the DTA curve of Al_2O_3-50 wt% TCP composites. This DTA curve is practically similar to the one shown in Figure 3b. Indeed, the DTA thermogram of the composites also shows two endothermic peaks. Figure 3 (d), (e) and (f) illustrate the DTA curves of Al_2O_3–40 wt% TCP composites, Al_2O_3–20 wt% TCP composites and Al_2O_3–10 wt% TCP composites, respectively. The DTA thermograms of each composites show only one endothermic peak between 1100°C and 1260°C, which are relative to the allotropic transformation of TCP (β to α). In these curves, we notice that the endothermic peak relative to a second allotropic transformation of TCP (α to α') has practically disappeared when the percentage of the alumina increases in the Al_2O_3 - TCP composites (Figure 3(d), (e) and (f)).
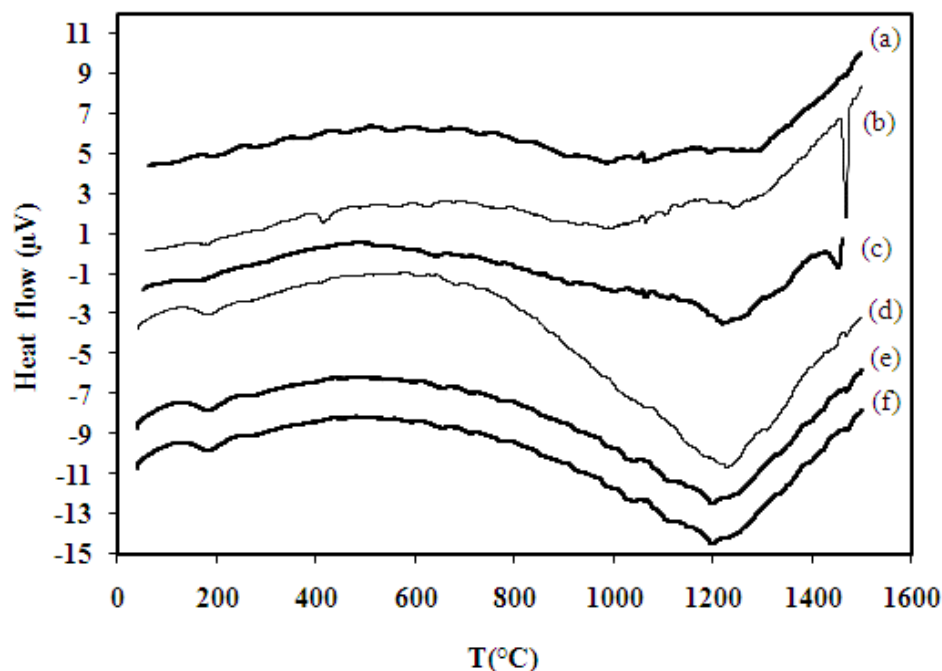
Figure 3. DTA curves of (a) α-Al$_2$O$_3$, (b) β-TCP, (c) Al$_2$O$_3$ – 50 wt% TCP composites, (d) Al$_2$O$_3$ – 40 wt% TCP composites, (e) Al$_2$O$_3$ – 20 wt% TCP composites and (f) Al$_2$O$_3$ – 10 wt% TCP composites

Figure 4 shows the dilatometric measurements of the different powders used in this study (β-TCP, α-Al$_2$O$_3$ and Al$_2$O$_3$ - TCP composites). A large sintering domain was observed for the three powders (β-TCP, alumina and composites). The sintering temperature of the initial powder began at about 900°C and at about 1400°C for the β-TCP and alumina (Figure 4a-b and Table 2). The sintering temperature of Al$_2$O$_3$-50 wt% TCP composites began at 1100°C (Figure 4c). It is to be noted that the presence of 50 wt% TCP in the alumina matrix decreases the sintering temperature of the alumina by around 300°C (Figure 4c). This variation of the sinterability is relative to the difference between the physicochemical compositions of these powders and the mixture of their different composites.

3.2. The mechanical properties of alumina–tricalcium phosphate composites

The influence of the sintering temperature on the rupture strength of Al$_2$O$_3$-TCP composites is shown in Figure 5. The mechanical resistance of Al$_2$O$_3$-TCP composites is studied at various temperatures (1400°C, 1450°C, 1500°C, 1550°C, 1600°C) for one hour with different percentages of β-TCP (50 wt%, 40 wt%, 20 wt% and 10 wt%). Thus, Figure 5 illustrates the rupture strength of the Al$_2$O$_3$-TCP composites relative to the percentages of the alumina and the sintering temperature. Consequently, the rupture strength of Al$_2$O$_3$ mixed with 10 wt% β-TCP reached its maximum value when sintered at 1600°C for one hour; it then decreased with the increase of this percentage. This is how the rupture strength of the Al$_2$O$_3$-10 wt% TCP composites reached 13.5 MPa.
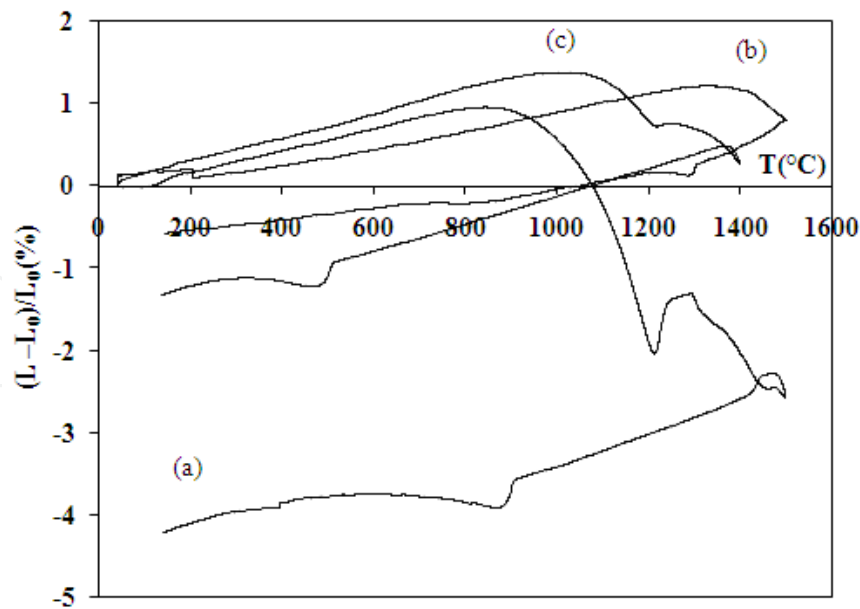
Figure 4. Linear shrinkage versus temperature of: (a) β-TCP, (b) α-Al_2O_3 and (c) Al_2O_3 – 50 wt% TCP composites
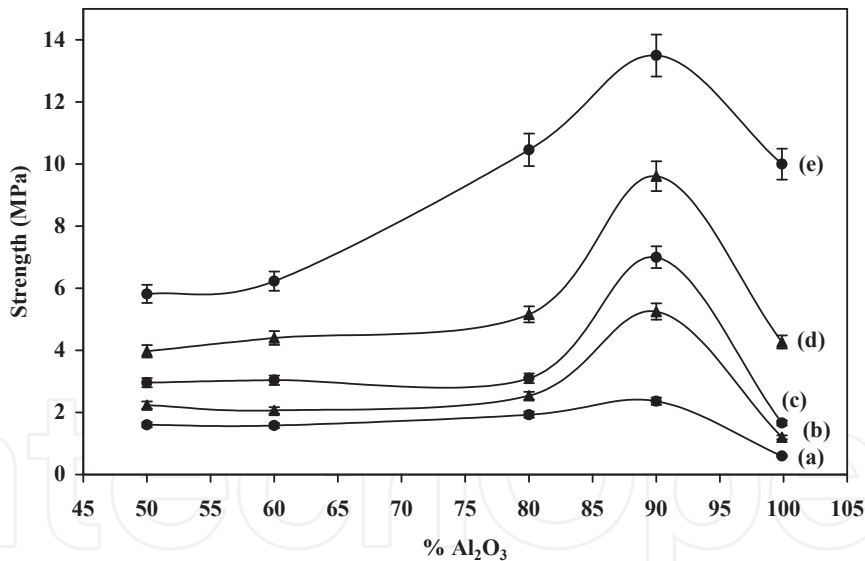

Figure 5. The rupture strength of the TCP-Al_2O_3 composites sintered for 1 hour at various temperatures: (a) 1400°C, (b) 1450°C, (c) 1500°C, (d) 1550°C and (e) 1600°C

Figure 6 shows the evolution of the rupture strength of the Al_2O_3 - 10 wt% TCP composites sintered at various temperatures (1500°C, 1550°C and 1600°C) for different sintering times (0 min, 30 min, 60 min and 90 min). The optimum value of the rupture strength was indeed obtained after an hour-long sintering process at 1600°C. Thus, the mechanical resistance of the samples reached 13.5 MPa.
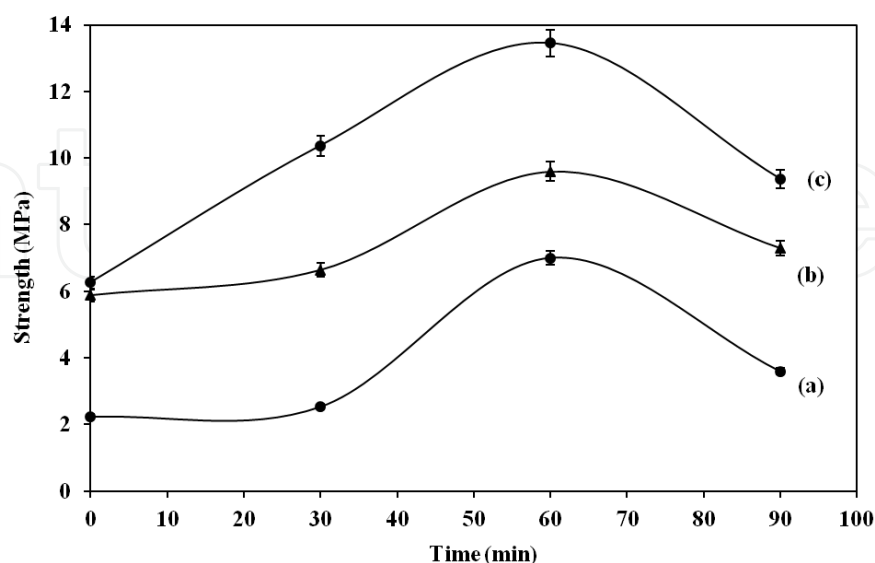
Figure 6. The rupture strength of the Al_2O_3–10 wt% TCP composites sintered for different lengths of time at various temperatures: (a) 1500°C, (b) 1550°C and (c) 1600°C

In this study, we showed that the presence of different amounts of alumina in the β-TCP improves the mechanical properties of Al_2O_3-TCP composites. In fact, the mechanical properties of Al_2O_3-10 wt% TCP composites reached the optimum value by being sintered at 1600°C for one hour. Thus, the rupture strength of these composites reached 13.5 MPa. Table 3 displays several examples of the mechanical properties of the calcium phosphates and the bone tissues. In comparison, we notice that the properties of Al_2O_3-10 wt% TCP composites are close to those of pure β-TCP, pure Fap and TCP-33.16 wt% Fap composites, which have a rupture strength of 5.3 MPa, 14 MPa and 13.7 MPa, respectively [15, 21, 25]. However, the mechanical properties of our composites are more closely comparable to those of the pure Fap and the TCP–33.16 wt% Fap composites (Table 3). Generally, the values found for the mechanical strength of our composites are not identical to those in Table 3, because the authors have used different mechanical modes other than the Brazilian test. In addition, many factors influence the mechanical properties of the samples such as: the use of particular initial powders as well as the conditions of the treatment process.

The sintering of materials is a complex process, involving the evolution of the microstructure through the action of several different transport mechanisms such as: surface diffusion, evaporation- condensation, grain boundary diffusion [3]. However, producing dense TCP–Al_2O_3 composites with a fine uniform microstructure through the sintering process does not seem to be a routine process because the β-TCP has a lower sinterability and a lower sintering temperature than those of pure alumina.

Materials	σ_r [a] (MPa)	σ_c [b] (MPa)	σ_f [c] (MPa)	References
β-TCP	4-6	-	92	[21,27]
Fap	10-14	-	-	[15]
Hap	-	5.35	-	[115]
TCP - 75 wt% Al_2O_3	8.60	-	-	[27]
TCP – 26.52 wt% Fap	9.60	-	-	[21]
TCP – 26.52 wt% Fap- 5 wt% Al_2O_3	13.60	-	-	[22]
TCP – 33.16 wt% Fap	13.70	-	-	[25]
Hap – TCP (40:60)	-	4.89	-	[115]
Al_2O_3 - 26.5 wt% Fap	21.7	-	-	[31]
Cortical bone	-	130-180	50-150	[1, 2]
Cancellous bone	-	2-12	-	[1, 2]

(a): Rupture strength (Brazilian test),

(b): compressive strength

(c): Flexural strength.

Table 3. Literature examples of the mechanical properties of calcium phosphates bioceramics and bone tissues

3.3. Characterization of alumina-tricalcium phosphate composites after the sintering process

Figure 7 shows the ^{31}P MAS-NMR spectra of the Al_2O_3-TCP composites obtained after the sintering process for 1 hour at 1550°C with different percentages of β-TCP (50 wt%, 40 wt%, 20 wt% and 10 wt%). The addition of 50 wt% Al_2O_3 to the TCP matrix shows the presence of several peaks which are assigned to the tetrahedral environment of P sites (1.03 ppm; 1.93 ppm; 3.50 ppm and 4.84 ppm) (Figure 7a). In fact, the increasing of the percentage of alumina in the TCP matrix decreases the number of the tetrahedral phosphorus site peaks which are reduced to a large single peak with 90 wt% alumina (Figure 7 b-d). Moreover, the tetrahedral environment of the phosphorus in tricalcium phosphate is not changed after the sintering process with different percentages of alumina. But the effect of the addition of alumina to the β-TCP matrix provokes the structural rearrangement of the coordination of phosphorus in β-TCP. Similar results were previously reported in literature [14, 26-27, 31].

The ^{27}Al MAS-NMR spectra of Al_2O_3-TCP composites sintered for 1 hour at 1550°C with different percentages of β-TCP (50 wt%, 40 wt%, 20 wt% and 10 wt%) are shown in Figure 8. The chemical shifts at 35 ppm and at 7.3 ppm indicate the presence of octahedral Al sites (Al[VI]) and pentahedral Al sites (Al[V]), respectively. The peak of pentahedral Al sites increases with the increase of the percentage of alumina in the Al_2O_3-TCP composites (Figure 8 b-8d). We notice especially the appearance of another octahedral Al peak at 18.6 ppm for alumina sintered with 40 wt% and 20 wt% of β-TCP (Figure 8 b-d). The aluminum in the alumina is

primarily in one pentahedral Al site (35 ppm) and in one octahedral Al site (7.3 ppm) (Figure 8e). For the alumina sintered with different percentages of β-TCP (50 wt%, 40 wt%, 20 wt% and 10 wt%), the spectra show two octahedral aluminum environments: AlO_6 at about 7.3 ppm and at 18.6 ppm (Fig 8b-d). Indeed, the intensity of the octahedral signal at 18.6 ppm increases with the percentage of alumina. The estimated concentrations of AlO_5 and AlO_6 are reported in Table 4. During the sintering process, the aluminum in the Al_2O_3-TCP composites provokes the structural rearrangement of the coordination of aluminum. Similar results were provisionally reported by different authors [22, 27, 31]. Indeed, these authors show that the coordination of the aluminum in octahedral sites was forced to change into another coordination in pentahedral sites [31]. The same authors point out that the structural rearrangement of the coordination of aluminum was probably produced by the formation of calcium aluminates which was produced after the sintering process and the reaction between calcium phosphates and alumina [31]. In conclusion, the ^{31}P magic angle scanning nuclear magnetic resonance analysis of different composites reveals the presence of tetrahedral P sites, while the [27]Al magic angle scanning nuclear magnetic resonance analysis shows the presence of both octahedral and pentahedral Al sites.
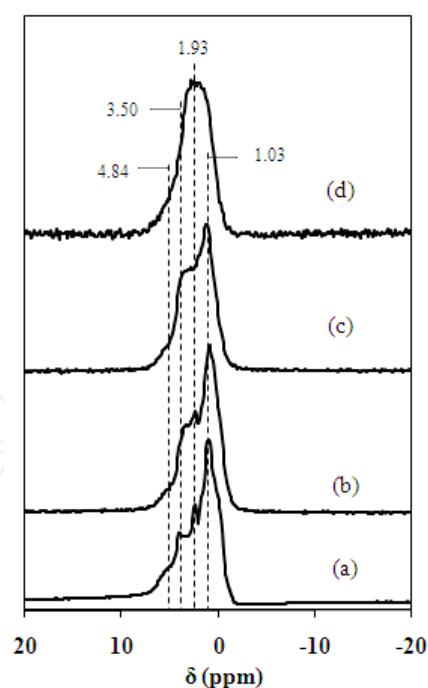

Figure 7. The ^{31}P MAS-NMR spectra of the Al_2O_3-TCP composites sintered for 1 hour at 1550°C with different percentages of β-TCP: (a) 50 wt%, (b) 40 wt%, (c) 20 wt% and (d) 10 wt%

Figure 8. The ^{27}Al MAS-NMR spectra of the Al_2O_3-TCP composites sintered for 1 hour at 1550°C with different percentages of β-TCP: (a) 50 wt%, (b) 40 wt%, (c) 20 wt%, (d) 10 wt% and (e) 0 wt%
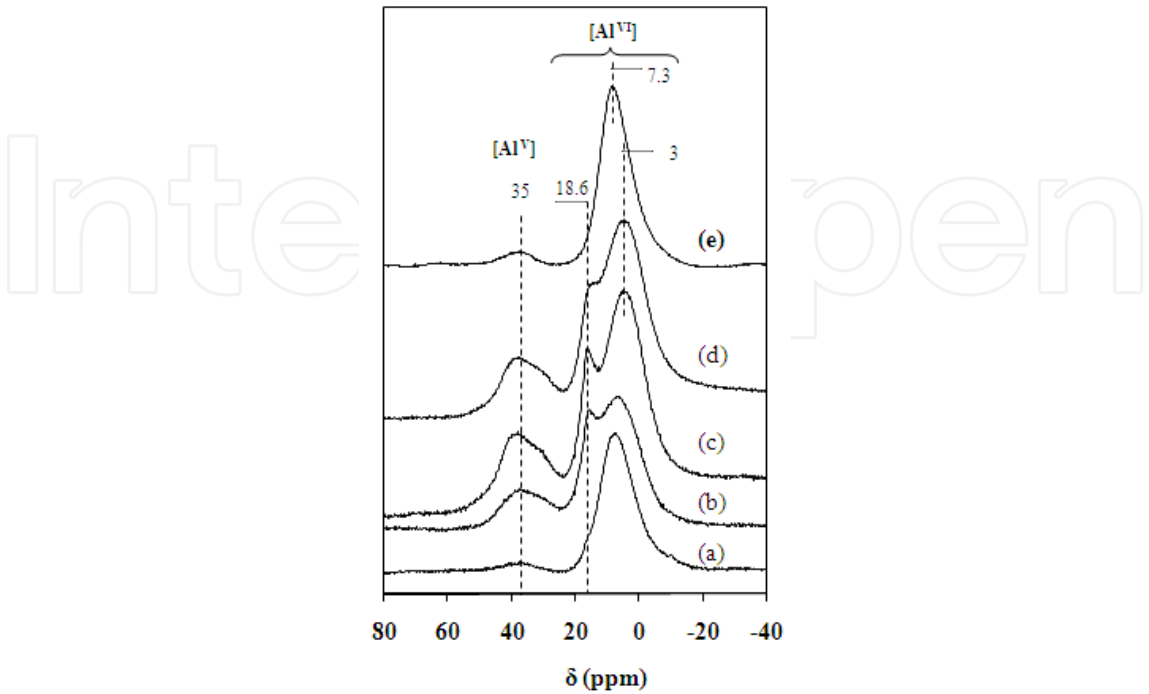
Compounds	AlO$_5$ (%)	AlO$_6$ (Type 1) (%)	AlO$_6$ (Type 2) (%)
δ (ppm)	30-40	7	18
TCP - 50 wt % Al$_2$O$_3$	0.50	99.50	
TCP - 60 wt % Al$_2$O$_3$	15.38	65.37	19.25
TCP - 80 wt % Al$_2$O$_3$	19.71	67.81	12.48
TCP- 90 wt % Al$_2$O$_3$	14.85	73.71	11.44
Al$_2$O$_3$	1.40	98.60	

Table 4. Properties of pentahedral and octahedral Al sites in the Al_2O_3-TCP composites sintered with different percentages of β-TCP at various temperatures for 1 hour

Figure 9 presents XRD patterns of Al_2O_3-TCP composites sintered at 1550°C for 1 hour with different percentages of β-TCP. Besides, the spectra show the characteristic peaks of β-TCP (ICDD data file no. 70-2065) and α- Al_2O_3 (ICDD data file no. 43-1484). This analysis shows that the peak of alumina is predominant in the elaboration of any composite.
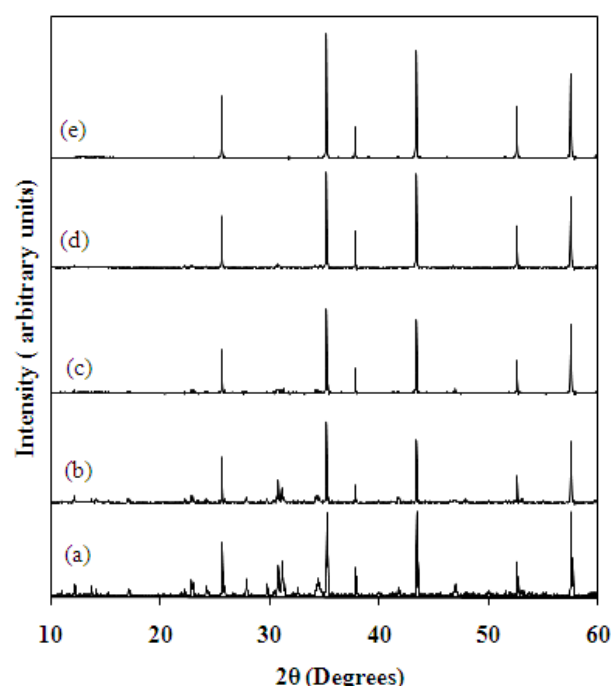
Figure 9. The XRD patterns of the Al_2O_3-TCP composites sintered at 1550°C for 1 hour with different percentages of β-TCP: (a) 50 wt%, (b) 40 wt%, (c) 20 wt%, (d) 10 wt% and (e) 0 wt%

The SEM technique helps to investigate the texture and porosity of any biomaterial. Figure 10 shows the fracture surface of the Al_2O_3-TCP composites sintered at 1550°C for 1 hour with different percentages of β-TCP. These micrographs show the coalescence between β-TCP grains produced with all the percentages of added alumina (Figure 10 a-d). The samples sintered with 50 wt%, 40 wt% and 20 wt% β-TCP present cracks and an important intragranular porosity (Figure 10 a-c). This result is a proof of the fragility of the composites elaborated with the different percentages of alumina as shown in Figure 10a-c. In fact, the microstructure of the composites shows different cracks relative to the allotropic transformation of TCP (β to α) (Figure 10 a-c). But the intensity of the cracks in the composites decreases with the increase in the percentage of β-TCP (Figure 10 a-d). Thus, the absence of micro-cracking and the reduction of the sizes of the pores in the Al_2O_3-10 wt% TCP composites explain the increase in the rupture strength of the samples (Figure 10 d_1-d_2). Indeed, the composites present excellent mechanical properties and a good aptitude for sinterability (Figure 10 d_1-d_2). The SEM micrographs of the alumina sintered without β-TCP shows an intergranular porosity (Figure 10e).

The effects of the sintering temperature on the microstructure of the Al_2O_3-10 wt% TCP composites are presented in Figure 11. The SEM micrographs show the coalescence between the grains with the increase of the sintering temperature. At 1500°C, the samples present an important intergranular porosity (Figure 11a). The microstructure of Al_2O_3-10 wt% TCP composites sintered at 1550°C shows a continuous phase relative to β-TCP phases and small-sized grains relative to the alumina phases (Figure 11b). Furthermore, at 1600°C, the boundaries between grains are evident in the micrographs (marked with arrows in Figure

11c), confirming the best mechanical resistance of Al_2O_3-10 wt% TCP composites in this temperature and with the addition of 10 wt% β-TCP (Figure 11c). In fact, the continuous phases in addition to the formed spherical pores prove that a liquid phase has appeared at 1600°C relative probably to the allotropic transformation of the β-TCP. This similar result was observed by Bouslama and colleagues [25].
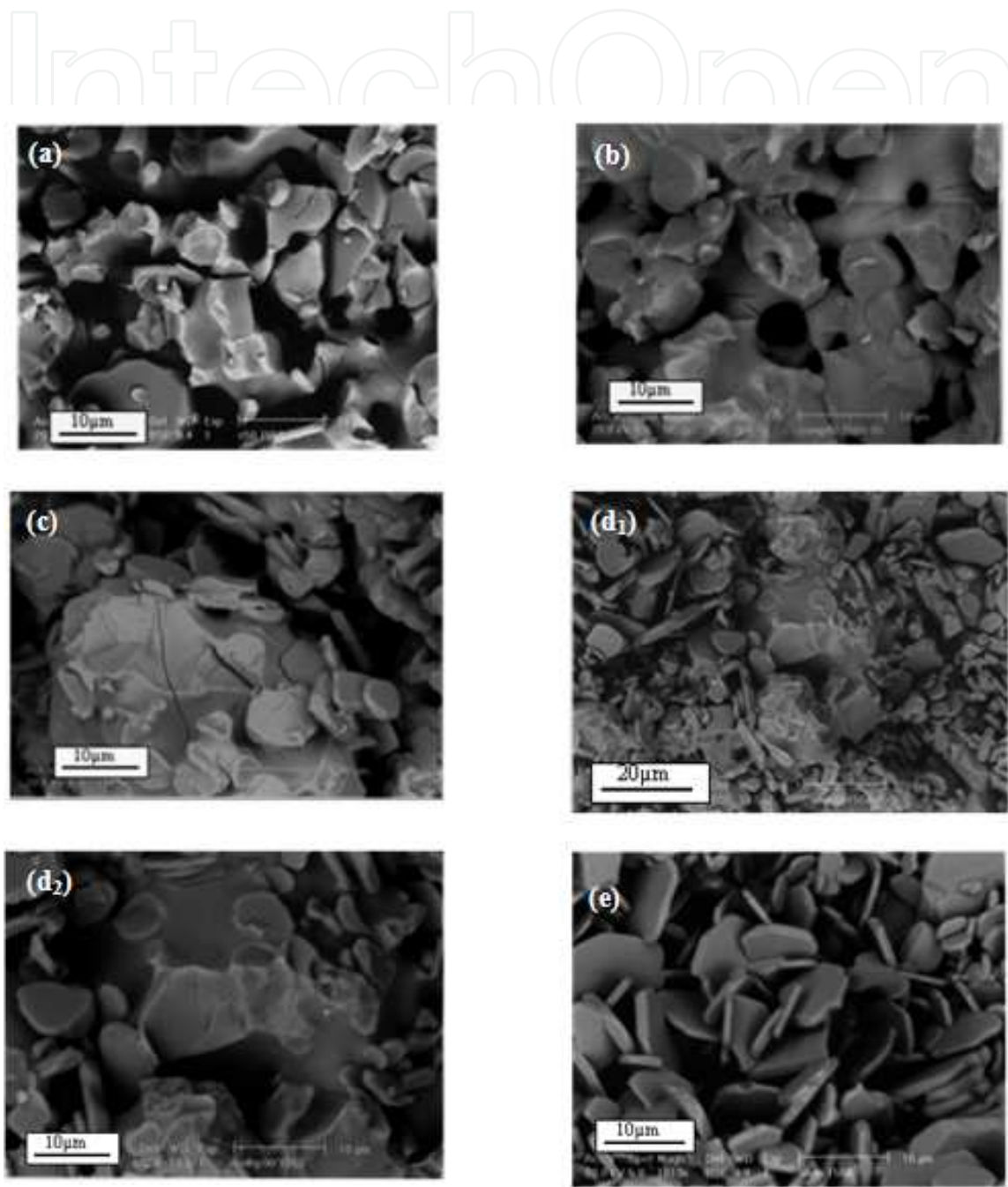
Figure 10. The SEM micrographs of the Al_2O_3 - TCP composites sintered at 1550°C for 1 hour with different percentages of β-TCP: (a) 50 wt%, (b) 40 wt%, (c) 20 wt%, (d_1-d_2) 10 wt% and (e) 0 wt%.
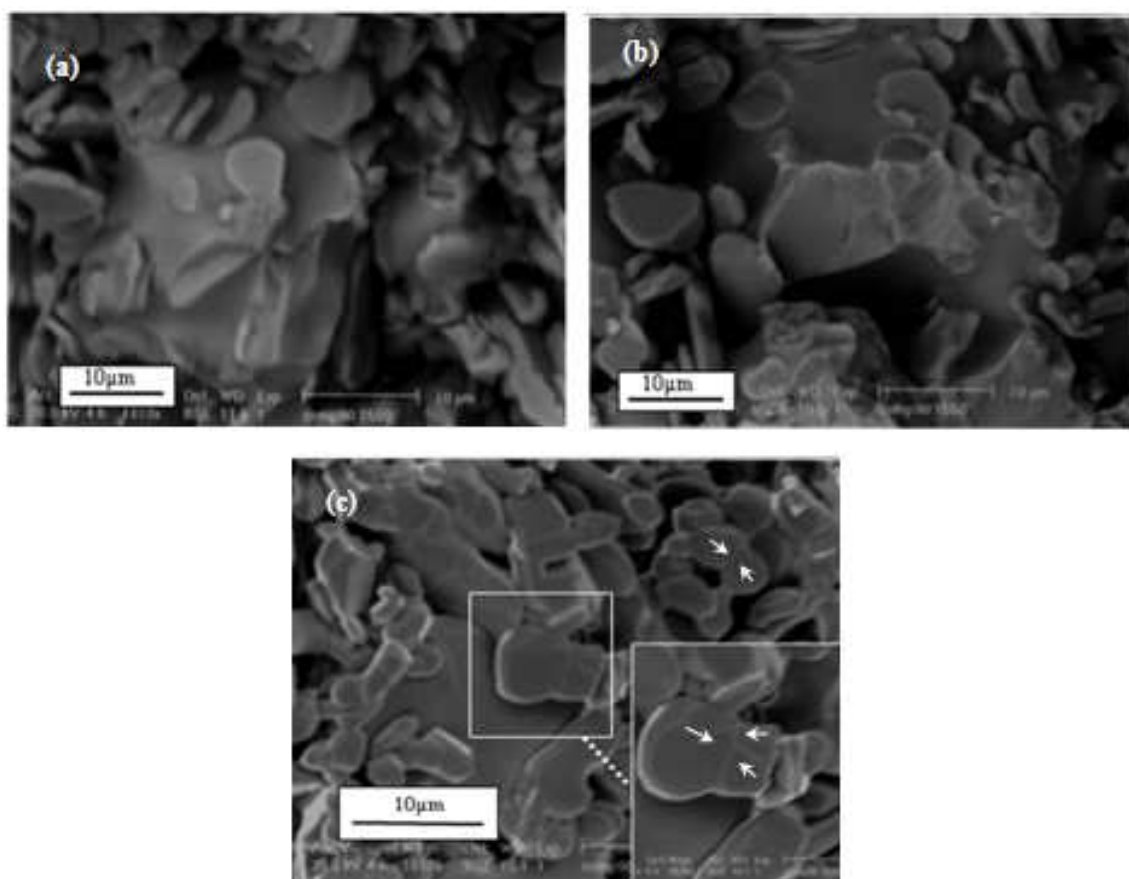
Figure 11. The SEM micrographs of the Al_2O_3-10 wt% TCP composites sintered for 1 hour at: (a) 1500°C, (b) 1550°C and (c) 1600°C.

The results of the microstructural investigations of Al_2O_3-10 wt% TCP composites sintered at 1600°C for different lengths of time (0 min, 30 min, 60 min and 90 min) are shown in Figure 12. These micrographs reveal the influence of different lengths of time on the microstructural developments during the sintering process at 1600°C. The microstructure of the samples leads to the formation of important cracks of different sizes with composites sintered for 0 min, 30 min and 90 min (Figure 12 ba-b and 12d). The continuous phases are relative to the β-TCP phase while the grains of a small size are relative to the alumina phase (Figure 12 ba-b and 12d). In Figure 12c, we notice the coalescence between the grains after the sintering process for 60 min confirming the best mechanical resistance in these conditions.

Furthermore, the sintering behavior of the Al_2O_3-TCP composites has been studied relative to the β-TCP content. It has been shown that alumina should be used in order to prevent the β-α transition of the tricalcium phosphate during the sintering process. At any rate, the results obtained in the present work would be valuable in the performance of Al_2O_3 - TCP composites resembling bone tissue engineering (Table 3). In fact, our preliminary tests indicated that the rupture strength of Al_2O_3-TCP composites is from 2 to 14 MPa. The optimum value of the Al_2O_3 - 10 wt% TCP composites sintered at 1600°C for one hour reached 13.5

MPa. This is true for the values of calcium phosphates fabricated by conventional techniques [116] and is close to a cancellous bone (2-12 MPa) [1-2, 117].
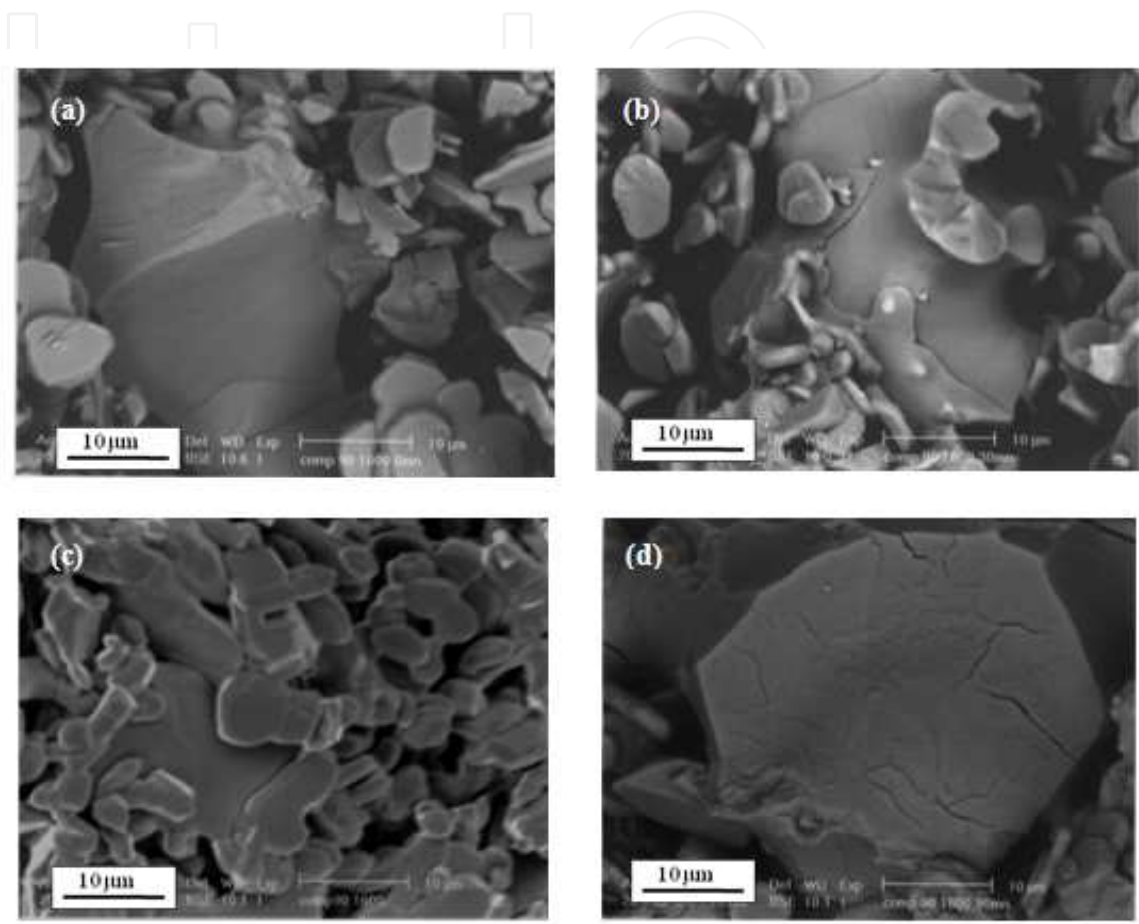

Figure 12. SEM micrographs of the Al_2O_3 - 10 wt% TCP composites sintered at 1600°C for: (a) 0 min, (b) 30 min, (c) 60 min and (d) 90 min.

According to the authors' best knowledge, the highest values of the mechanical characteristics for different samples are detailed in Table 3. As it can be seen from this table, the various techniques used to prepare dense sintered bioceramics affect the final density, as well as the composition of the phase and, consequently, the final mechanical properties of samples. The Al_2O_3 - 10 wt% TCP composites show high rupture strength, which is in concordance with the other results [10, 15, 21, 25-27, 29]. The rupture strength obtained for TCP-Al_2O_3 composites is from 2 to 14 MPa, within the values reported in the literature (Table 3). Moreover, the wide variation in the reported rupture strength of the composites is due to the synthesis

route of the β-TCP powder, the size of its particle as well as to its density; it is also due to the application of different processing parameters.

At first, the objective of this work was to characterize the mechanical properties of alumina – TCP composites produced after the sintering process. A sintering stage appears to be of great importance to produce biomaterials with the required properties. Several processes occur during the sintering process of tricalcium phosphate and bioinert oxide. Firstly, the TCP powders are synthesized by solid reaction. Secondly, alumina – TCP powders are sintered for production of dense bioceramics with subsequent shrinkage of the samples. Thirdly, the mechanical properties of alumina–TCP composites are accompanied by a concurrent increase in grain size and a formation of cracks in the alumina sintered with different percentages of TCP (20 wt%, 40 wt% and 50 wt%). Besides, sintering causes the toughening and the increase of the mechanical strength of alumina–10 wt% TCP composites. An extensive study on the effect of the sintering temperature and time on the properties of alumina–TCP composites revealed a correlation between these parameters and density, porosity, grain size, chemical composition and strength of different composites. The degree of densification and mechanical properties of alumina–TCP composites appeared to depend on the sintering temperature and the duration of sintering. Alumina–TCP powders can be pressed and sintered up to theoretical density at 1400°C–1600°C. Processing them with higher percentage of TCP (20 wt%, 40 wt% and 50 wt%) may lead to exaggerated grain growth and formation of cracks because of the formation of α-TCP at higher temperatures. Indeed, the allotropic transformation of TCP is a function of the sintering temperature. The presence of cracks in the alumina–TCP composites is reported to inhibit the mechanical properties. A definite correlation between mechanical strength and grain size in sintered alumina–TCP composites was found: the strength started to decrease at lower sintering temperature and with higher percentage of TCP (20 wt%, 40 wt% and 50 wt%). The sintering process of alumina – 10 wt% TCP composites makes it possible to decrease the grain size and achieve higher densities. This leads to finer microstructures, higher thermal stability of alumina–10 wt% TCP composites and subsequently better mechanical properties of the prepared bioceramics composites. The mechanical properties of alumina – TCP composites is from 2 to 14 MPa. Generally, the mechanical properties of samples increase with the decrease in grain size. In fact, the mechanical strength of alumina–10 wt% TCP composites reaches a maximum value with the decrease in the size of the grains of composites. The optimum measured value of the strength of the alumina–10 wt% TCP composites was 13.5 MPa. This value is compared to those of cancellous bone. Similar values for porous HAp are in the ranges of 2-10 MPa [118]. Generally, variations of mechanical properties of samples are caused by a statistical nature of the strength distribution, influence of remaining microporosity, grain size, presence of impurities and Ca/P ratio [118].

In conclusion, an interfacial reaction between β-TCP and alumina has been studied in the nanocomposites of Al_2O_3-TCP. It was found that the alumina did not completely react with the β-TCP and did not form calcium aluminates. Moreover, it has been shown that the alumina prevents the formation of cracks in the microstructure of composites containing 10 wt % of β-TCP. The mechanical characteristics should be taken into consideration in order to

better assess the relationship between the processing conditions, the microstructural design as well as the mechanical response.

4. Conclusions

The biomaterials of alumina-tricalcium phosphate composites have been characterized by using MAS NMR, XRD and SEM analysis after the sintering process. The effect of β-TCP additive on the alumina matrix was observed in different thermal analyses: dilatometry analysis and DTA analysis. The mechanical properties have been investigated by the Brazilian test. This investigation has allowed us to define the sintering temperature and the percentage of added alumina for which β-TCP should have an optimal densification and better mechanical properties. This study has also allowed us to summarize the effect of the sintering temperature and the length of sintering time on the mechanical properties of the Al_2O_3-TCP composites. The produced Al_2O_3-TCP composites with different percentages of β-TCP (50 wt%; 40 wt%; 20 wt% and 10 wt%) exhibited much better mechanical properties than the reported values of β-TCP without alumina. The Al_2O_3-TCP composites showed a higher rupture strength at 1600°C, which certainly increased with the alumina content and reached the optimum value with 90 wt%. However, no cracks were observed in the microstructure of the composites which contained this percentage of alumina. This is due to the allotropic transformation of the tricalcium phosphate. The partial or reversal transformation of tricalcium phosphate (β to α or α to α′) during the cooling period could induce a residual stress within the dense bioceramics, marking it much more brittle. Accordingly, the optimum performance of alumina-tricalcium phosphate composites achieved 13.5 MPa. Furthermore, the best mechanical properties of the composites were obtained after the sintering process at 1600°C for 1 hour. With different weight rations of tricalcium phosphate: alumina (50:50, 40:60 and 20:80), the performance of the composites was hindered by the formation of both cracks and intragranular porosity.

Acknowledgements

Author details

Siwar Sakka, Jamel Bouaziz and Foued Ben Ayed[*]

*Address all correspondence to: benayedfoued@yahoo.fr

Laboratory of Industrial Chemistry, National School of Engineering, Sfax University, Sfax, Tunisia

References

[1] Hench L L. Bioceramics: From Concept to clinic. J. Am. Ceram. Soc. 1991; 74 (7) 1487.

[2] Hench L L. An Introduction to Bioceramics. J. Wilson (ed.). Vol. 1. World Scientific, Singapore; 1993.

[3] Elliott J C. Structure and Chemistry of the Apatite and Other Calcium Orthophosphates. Amsterdam : Elsevier Science B.V.; 1994.

[4] Landi E, Tampieri A, Celotti G, Sprio S. Densification behaviour and mechanisms of synthetic hydroxyapatites. J. Eur. Ceram. Soc. 2000; 20, 2377.

[5] Ben Ayed F, Bouaziz J, Bouzouita K. Pressureless sintering of fluorapatite under oxygen atmosphere. J. Eur. Ceram. Soc. 2000; 20 (8) 1069.

[6] Ben Ayed F, Bouaziz J, Khattech I, Bouzouita K. Produit de solubilité apparent de la fluorapatite frittée. Ann. Chim. Sci. Mater. 2001; 26 (6) 75.

[7] Ben Ayed F, Bouaziz J, Bouzouita K. Calcination and sintering of fluorapatite under argon atmosphere. J. Alloys Compd. 2001; 322 (1-2) 238.

[8] Varma H K, Sureshbabu S. Oriented growth of surface grains in sintered b tricalcium phosphate bioceramics. Materials letters 2001; 49, 83.

[9] Destainville A, Champion E, Bernache – Assolant D. Synthesis. Characterization and thermal behavior of apatitic tricalcium phosphate. Mater. Chem. Phys. 2003; 80, 269.

[10] Wang C X, Zhou X, Wang M. Influence of sintering temperatures on hardness and Young's modulus of tricalcium phosphate bioceramic by nanoindentation technique. Materials Characterization 2004; 52, 301.

[11] Hoell S, Suttmoeller J, Stoll V, Fuchs S, Gosheger G. The high tibial osteotomy, open versus closed wedge, a comparison of methods in 108 patients. Arch.Trauma Surg. 2005; 125, 638–43.

[12] Gaasbeek R D, Toonen H G, Van Heerwaarden R J, Buma P. Mechanism of bone incorporation of β-TCP bone substitute in open wedge tibial osteotomy in patients. Biomaterials 2005; 26, 6713–6719.

[13] Jensen S S, Broggini N, Hjorting-Hansen E, Schenk R, Buser D. Bone healing and graft resorption of autograft, anorganic bovine bone and beta-tricalcium phosphate. A histologic and histomorphometric study in the mandibles of minipigs.. Clin. Oral. Implants Res. 2006; 17, 237–243.

[14] Ben Ayed F, Chaari K, Bouaziz J, Bouzouita K. Frittage du phosphate tricalcique. C. R. Physique, 2006; 7 (7) 825.

[15] Ben Ayed F, Bouaziz J, Bouzouita K. Résistance mécanique de la fluorapatite. Ann. Chim. Sci. Mater. 2006; 31 (4) 393.

[16] Gutierres M, Dias A G, Lopes M A, Hussain N S, Cabral A T, Almeid L. Opening wedge high tibial osteotomy using 3D biomodelling Bone like macroporous structures: case report. J. Mater. Sci. Mater. Med. 2007; 7 (18) 2377–2382.

[17] DeSilva G L, Fritzler A, DeSilva S P. Antibiotic-impregnated cement spacer for bone defects of the forearm and hand. Tech. Hand Up Extrem Surg. 2007; 11, 163–7

[18] Ben Ayed F, Bouaziz J. Élaboration et caractérisation d'un biomatériau à base de phosphates de calcium. C. R. Physique, 2007; 8 (1) 101-108.

[19] Ben Ayed F, Bouaziz J. Sintering of tricalcium phosphate–fluorapatite composites by addition of alumina. Ceramics Int. 2008; 34 (8) 1885-1892.

[20] Ben Ayed F, Bouaziz J. Sintering of tricalcium phosphate–fluorapatite composites with zirconia. J. Eur. Ceram. Soc., 2008; 28 (10) 1995-2002.

[21] Bouslama N, Ben Ayed F, Bouaziz J. Sintering and mechanical properties of tricalcium phosphate–fluorapatite composites. Ceramics Int. 2009; 35, 1909-1917.

[22] Bouslama N, Ben Ayed F, Bouaziz J. Mechanical properties of tricalcium phosphate-fluorapatite-alumina composites. Physics Procedia 2009; 2, 1441-1448.

[23] Chaari K, Ben Ayed F, Bouaziz J, Bouzouita K. Elaboration and characterization of fluorapatite ceramic with controlled porosity. Materials Chemistry and Physics 2009; 113, 219-226.

[24] Guha A K, Singh S, Kumarresan R, Nayar S, Sinha A. Mesenchymal cell response to nanosized biphasic calcium phosphate composites. Coll. Surf. B biointerface 2009; 73, 146-51.

[25] Bouslama N, Ben Ayed F, Bouaziz J. Effect of fluorapatite additive on densification and mechanical properties of tricalcium phosphate. J. Mechanical Behaviour of Biomedical Materials 2010; 3, 2-13.

[26] Ben Ayed F. Biomaterials - Physics and Chemistry, Chapter 18: Elaboration and characterisation of calcium phosphate biomaterial for biomedical application, ISBN 978-953-307-418-4. Croatia: In Tech; 2011. p 357 – 374.

[27] Sakka S, Ben Ayed F, Bouaziz J. Mechanical properties of tricalcium phosphate–alumina composites. IOP Conf. Series : Materials Science and Engineering, 2012. 28, 012028

[28] Sellami I, Ben Ayed F, Bouaziz J. Effect of fluorapatite additive on the mechanical properties of tricalcium phosphate-zirconia composites. IOP Conf. Series : Materials Science and Engineering, 2012. 28, 012029.

[29] Ben Ayed F. Current microscopy contributions to advances in science and technology, Chapter: The effect of the sintering process on the microstructure and the mechanical properties of biomaterials. published by Formatex Research Center Spain; to be published in 2012.

[30]   Levin I, Brandon D. Metastable Alumina Polymorphs: Crystal Structures and Transi‐
       tion. Sequences. J. Am. Ceram. Soc. 1998, 81.

[31]   Guidera A, Chaari K, Bouaziz J. Elaboration and Characterization of Alumina-Fluo‐
       rapatite Composites. J. Biomat. Nano. 2011; 2, 103-113.

[32]   Doremus RH. Bioceramics. J Mater Sci 1992; 27, 285–97.

[33]   Vallet-Regı́ M. Ceramics for medical applications. J Chem Soc Dalton Trans 2001,
       97–108.

[34]   Rahaman MN, Yao A, Bal BS, Garino JP, Ries MD. Ceramics for prosthetic hip and
       knee joint replacement. J Am Ceram Soc 2007; 90, 1965–88.

[35]   Best SM, Porter AE, Thian ES, Huang J. Bioceramics: past, present and for the future.
       J Eur Ceram Soc 2008; 28, 1319–27.

[36]   Lowenstam HA, Weiner S. On biomineralization. Oxford University Press, 1989; pp
       324.

[37]   LeGeros RZ. Calcium phosphates in oral biology and medicine. Basel: Karger; 1991,
       201.

[38]   Weiner S, Wagner HD. Material bone: structure-mechanical function relations. Ann
       Rev Mater Sci 1998; 28, 271–98.

[39]   Weiner S, Traub W, Wagner HD. Lamellar bone: structure-function relations. J Struct
       Biol 1999; 126, 241–55.

[40]   Weiner S, Dove PM. An overview of biomineralization processes and the problem of
       the vital effect. In: Dove PM, de Yoreo JJ, Weiner S, editors. Biomineralization, series:
       reviews in mineralogy and geochemistry, vol. 54. Washington, D.C., USA: Minera‐
       logical Society of America; 2003. p 1–29.

[41]   Albee FH. Studies in bone growth – triple calcium phosphate as stimulus to osteo‐
       genesis. Ann Surg 1920; 71, 32–9.

[42]   Nery EB, Lynch KL, Hirthe WM, Mueller KH. Bioceramic implants in surgically pro‐
       duced infrabony defects. J Periodontol 1975; 46, 328–47.

[43]   Denissen HW, de Groot K. Immediate dental root implants from synthetic dense cal‐
       cium hydroxylapatite. J Prosthet Dent 1979; 42, 551–6.

[44]   Levitt GE, Crayton PH, Monroe EA, Condrate RA. Forming methods for apatite
       prosthesis. J Biomed Mater Res 1969; 3, 683–5.

[45]   Blakeslee KC, Condrate Sr RA. Vibrational spectra of hydrothermally prepared hy‐
       droxyapatites. J Am Ceram Soc 1971; 54, 559–63.

[46]   Garrington GE, Lightbody PM. Bioceramics and dentistry. J Biomed Mater Res 1972;
       6, 333–43.

[47] Cini L, Sandrolini S, Paltrinieri M, Pizzoferrato A, Trentani C. Materiali bioceramici in funzione sostitutiva. Nota preventiva. (Bioceramic materials for replacement purposes. Preliminary note.). La Chirurgia Degli Organi Di Movimento 1972; 60, 423–30.

[48] Hulbert SF, Young FA, Mathews RS, Klawitter JJ, Talbert CD, Stelling FH. Potential of ceramic materials as permanently implantable skeletal prostheses. J Biomed Mater Res 1970; 4, 433–56.

[49] Hench LL, Splinter RJ, Allen WC, Greenlee TK. Bonding mechanisms at the interface of ceramic prosthetic materials. J Biomed Mater Res 1971; 2, 117–41.

[50] Hulbert SF, Hench LL, Forces D, Bowman L. History of bioceramics. In: Vincenzini P, editor. Ceramics in surgery. Amsterdam, The Netherlands: Elsevier, 1983; p 3–29.

[51] Jarcho M. Calcium phosphate ceramics as hard tissue prosthetics. Clin Orthop Relat Res 1981; 157, 259–78.

[52] de Groot K. Bioceramics consisting of calcium phosphate salts. Biomaterials 1980; 1 (1) 47–50.

[53] Aoki H, Kato KM, Ogiso M, Tabata T. Studies on the application of apatite to dental materials. J Dent Eng 1977; 18, 86–9.

[54] Roy DM, Linnehan SK. Hydroxyapatite formed from coral skeletal carbonate by hydrothermal exchange. Nature 1974; 247, 220–2.

[55] Holmes RE. Bone regeneration within a coralline hydroxyapatite implant. Plast Reconstr Surg 1979; 63, 626–33.

[56] Elsinger EC, Leal L. Coralline hydroxyapatite bone graft substitutes. J Foot Ankle Surg 1996; 35, 396–9.

[57] LeGeros RZ, LeGeros JP. Calcium phosphate bioceramics: past, present, future. Key Eng Mater 2003; 240–242, 3–10.

[58] Durucan C, Brown PW. Low temperature formation of calcium-deficient hydroxyapatite-PLA/PLGA composites. J Biomed Mater Res 2000; 51A, 717–25.

[59] Ginebra MP, Rilliard A, Ferna´ndez E, Elvira C, Roma´n JS, Planell JA. Mechanical and rheological improvement of a calcium phosphate cement by the addition of a polymeric drug. J Biomed Mater Res 2001; 57, 113–8.

[60] Yokoyama A, Yamamoto S, Kawasaki T, Kohgo T, Nakasu M. Development of calcium phosphate cement using chitosan and citric acid for bone substitute materials. Biomaterials 2002; 23, 1091–101.

[61] Barralet JE, Gaunt T, Wright AJ, Gibson IR, Knowles JC. Effect of porosity reduction by compaction on compressive strength and microstructure of calcium phosphate cement. J Biomed Mater Res 2002; 63B, 1–9.

[62] Bohner M, Gbureck U, Barralet JE. Technological issues for the development of more efficient calcium phosphate bone cements: a critical assessment. Biomaterials 2005; 26, 6423–9.

[63] Bohner M, Baroud G. Injectability of calcium phosphate pastes. Biomaterials 2005; 26, 1553–63.

[64] Link DP, van den Dolder J, van den Beucken JJ, Wolke JG, Mikos AG, Jansen JA. Bone response and mechanical strength of rabbit femoral defects filled with injectable CaP cements containing TGF-b1 loaded gelatin microspheres. Biomaterials 2008; 29, 675–82.

[65] Friedman CD, Costantino PD, Takagi S, Chow LC. Bone source hydroxyapatite cement: a novel biomaterial for craniofacial skeletal tissue engineering and reconstruction. J Biomed Mater Res 1998; 43B, 428–32.

[66] Shindo ML, Costantino PD, Friedman CD, Chow LC. Facial skeletal augmentation using hydroxyapatite cement. Arch Otolaryngol Head Neck Surg 1993; 119, 185–90.

[67] Chow LC. Calcium phosphate cements: chemistry, properties, and applications. Mat Res Soc Symp Proc 2000; 599, 27–37.

[68] Muzzarelli RAA, Biagini G, Bellardini M, Simonelli L, Castaldini C, Fraatto G. Osteoconduction exerted by methylpyrolidinone chitosan in dental surgery. Biomaterials 1993; 14, 39–43.

[69] Hing KA, Best SM, Bonfield W. Characterization of porous hydroxyapatite. J Mater Sci Mater Med 1999; 10, 135–45.

[70] Jordan DR, Gilberg S, Bawazeer A. Coralline hydroxyapatite orbital implant (Bio-Eye): experience with 158 patients. Ophthal Plast Reconstr Surg 2004; 20, 69–74.

[71] Yoon JS, Lew H, Kim SJ, Lee SY. Exposure rate of hydroxyapatite orbital implants a 15-year experience of 802 cases. Ophthalmology 2008; 115, 566–72.

[72] Schnettler R, Stahl JP, Alt V, Pavlidis T, Dingeldein E, Wenisch S. Calcium phosphate-based bone substitutes. Eur J Trauma 2004; 4, 219–29.

[73] Zyman ZZ, Glushko V, Dedukh N, Malyshkina S, Ashukina N. Porous calcium phosphate ceramic granules and their behaviour in differently loaded areas of skeleton. J Mater Sci Mater Med 2008; 19, 2197–205.

[74] Larsson S, Hannink G. Injectable boneegraft substitutes: current products, their characteristics and indications, and new developments. Injury 2011; 42, 30e4.

[75] Dorozhkin SV. Calcium orthophosphate cements for biomedical application. J Mater Sci 2008; 43, 3028e57.

[76] Dorozhkin SV. Calcium orthophosphate-based biocomposites and hybrid biomaterials. J Mater Sci 2009; 44, 2343e87.

[77] Bohner M, Gbureck U, Barralet JE. Technological issues for the development of more efficient calcium phosphate bone cements: a critical assessment. Biomaterials 2005; 26, 6423e9.

[78] Von Gonten AS, Kelly JR, Antonucci JM. Load-bearing behavior of a simulated craniofacial structure fabricated from a hydroxyapatite cement and bioresorbable fiber mesh. J Mater Sci Mater Med 2000; 11, 95e100.

[79] Canal C, Ginebra MP. Fibre-reinforced calcium phosphate cements: a review. J Mech Behav Biomed Mater 2011; 4, 1658e71.

[80] Callister Jr WD, Rethwisch DG. Materials science and engineering: an introduction. Hoboken: John Wiley Sons Inc; 2009.

[81] LeGeros RZ. Biodegradation and bioresorption of calcium phosphate ceramics. Clin Mater 1993;14, 65–88.

[82] Suchanek W, Yoshimura M. Processing and properties of hydroxyapatitebased biomaterials for use as hard tissue replacement implants. J Mater Res 1998; 13, 94–117.

[83] Hing KA, Best SM, Bonfield W. Characterization of porous hydroxyapatite. J Mater Sci Mater Med 1999; 10, 135–45.

[84] Ducheyne P, Qiu Q. Bioactive ceramics: the effect of surface reactivity on bone formation and bone cell function. Biomaterials 1999; 20, 2287–303.

[85] Pilliar RM, Filiaggi MJ, Wells JD, Grynpas MD, Kandel RA. Porous calcium polyphosphate scaffolds for bone substitute applications – in vitro characterization. Biomaterials 2001; 22, 963–72.

[86] Chu TMG, Orton DG, Hollister SJ, Feinberg SE, Halloran JW. Mechanical and in vivo performance of hydroxyapatite implants with controlled architectures. Biomaterials 2002; 23, 1283–93.

[87] Hench LL, Polak JM. Third-generation biomedical materials. Science 2002; 295, 1014–7.

[88] Tamai N, Myoui A, Tomita T, Nakase T, Tanaka J, Ochi T, et al. Novel hydroxyapatite ceramics with an interconnective porous structure exhibit superior osteoconduction in vivo. J Biomed Mater Res 2002; 59, 110–7.

[89] Simon JL, Roy TD, Parsons JR, Rekow ED, Thompson VP, Kemnitzer J, et al. Engineered cellular response to scaffold architecture in a rabbit trephine defect. J Biomed Mater Res 2003; 66A, 275–82.

[90] Deville S, Saiz E, Nalla RK, Tomsia AP. Freezing as a path to build complex composites. Science 2006; 311, 515–8.

[91] Miranda P, Pajares A, Saiz E, Tomsia AP, Guiberteau F. Fracture modes under uniaxial compression in hydroxyapatite scaffolds fabricated by robocasting. J Biomed Mater Res 2007; 83A, 646–55.

[92] Miranda P, Pajares A, Saiz E, Tomsia AP, Guiberteau F. Mechanical properties of calcium phosphate scaffolds fabricated by robocasting. J Biomed Mater Res 2008; 85A, 218–27.

[93] Brown WE, Chow LC. A new calcium phosphate water setting cement. In: Brown PW, editor. Cements research progress. Westerville, OH: Am Ceram Soc; 1986. p 352–79.

[94] Daculsi G, Weiss P, Bouler JM, Gauthier O, Millot F, Aguado E. Biphasic calcium phosphate/hydrosoluble polymer composites: a new concept for bone and dental substitution biomaterials. Bone 1999; 25 (Suppl. 2), 59S–61S.

[95] Alam I, Asahina I, Ohmamiuda K, Enomoto S. Comparative study of biphasic calcium phosphate ceramics impregnated with rhBMP-2 as bone substitutes. J Biomed Mater Res 2001; 54, 129–38.

[96] Daculsi G, Laboux O, Malard O, Weiss P. Current state of the art of biphasic calcium phosphate bioceramics. J Mater Sci Mater Med 2003; 14, 195–200.

[97] Daculsi G. Biphasic calcium phosphate granules concept for injectable and mouldable bone substitute. Adv Sci Technol 2006; 49, 9–13.

[98] LeGeros RZ, Lin S, Rohanizadeh R, Mijares D, LeGeros JP. Biphasic calcium phosphate bioceramics: preparation, properties and applications. J Mater Sci Mater Med 2003;14, 201–9.

[99] Lecomte A, Gautier H, Bouler JM, Gouyette A, Pegon Y, Daculsi G, et al. Biphasic calcium phosphate: a comparative study of interconnected porosity in two ceramics. J Biomed Mater Res B (Appl Biomater) 2008; 84B, 1–6.

[100] Tancret F, Bouler JM, Chamousset J, Minois LM. Modelling the mechanical properties of microporous and macroporous biphasic calcium phosphate bioceramics. J Eur Ceram Soc 2006; 26, 3647–56.

[101] Langstaff SD, Sayer M, Smith TJN, Pugh SM. Resorbable bioceramics based on stabilized calcium phosphates. Part II: evaluation of biological response. Biomaterials 2001; 22, 135–50.

[102] Sayer M, Stratilatov AD, Reid JW, Calderin L, Stott MJ, Yin X, et al. Structure and composition of silicon-stabilized tricalcium phosphate. Biomaterials 2003; 24, 369–82.

[103] Yin X, Stott MJ, Rubio A. a- and b-tricalcium phosphate: a density functional study. Phys Rev B 2003; 68, 205205.

[104] Yin X, Stott MJ. Theoretical insights into bone grafting Si-stabilized a-tricalcium phosphate. J Chem Phys 2005; 122, 024709.

[105] Reid JW, Pietak AM, Sayer M, Dunfield D, Smith TJN. Phase formation and evolution in the silicon substituted tricalcium phosphate/apatite system. Biomaterials 2005; 26, 2887–97.

[106] Yin X, Stott MJ. Surface and adsorption properties of a-tricalcium phosphate. J Chem Phys 2006;124, 124701.

[107] Ruan JM, Zou JP, Zhou JN, Hu JZ. Porous hydroxyapatite – tricalcium phosphate bioceramics. Powder Metall 2006; 49, 66–9.

[108] Reid JW, Tuck L, Sayer M, Fargo K, Hendry JA. Synthesis and characterization of single-phase silicon substituted a-tricalcium phosphate. Biomaterials 2006; 27, 2916–25.

[109] da Silva RV, Bertran CA, Kawachi EY, Camilli JA. Repair of cranial bone defects with calcium phosphate ceramic implant or autogenous bone graft. J Craniofac Surg 2007; 18, 281–6.

[110] O'Neill WC. The fallacy of the calcium – phosphorus product. Kidney Int 2007; 72, 792–6.

[111] Sanchez-Saʹlcedo S, Arcos D, Vallet-Regıʹ M. Upgrading calcium phosphate scaffolds for tissue engineering applications. Key Eng Mater 2008; 377, 19–42.

[112] Brunauer S, Emmet P H, Teller. Adsorption of Gases in Multimolecular Layers. J. Amer. Chem. Soc. J. 1938; 60, 310.

[113] ISRM. Suggested methods for determining tensile strength of rock materials, Int. J. Rock Mech. Min. Sci. Geomech. Abstr. 1978; 15, 99.

[114] ASTM C496, Standard test method for splitting tensile strength of cylindrical concrete specimens Annual Book of ASTM, Standards, vol. 0.042, ASTM, Philadelphia, 1984; p 336.

[115] Balcik C, Tokdemir T, Senkoylo A, Koc N, Timucin M, Akin S, Korkusuz P, Korkusuz F. Early weight bearing of porous HA/TCP (60/40) ceramics in vivo: a longitudinal study in a segmental bone defect model of rabbit. Acta Biomaterialia 2007; 3, 985-996.

[116] Deville S, Saiz E, Nalla RK, Tomsia A P. Freezing as a path to build complex composites. Science. 2006; 311 (5760) 515-518.

[117] Murugan R, Ramakrishna S. Development of nanocomposites for bone grafting. Compos Sci Technol. 2005; 65 (15-16) 2385-2406.

[118] Suchanek WL, Yoshimura M. Processing and properties of hydroxyapatite based biomaterials for use as hard tissue replacement implants. J Mater Res 1998; 13, 94–117.